Journal of Hydrology 618 (2023) 129192

Contents lists available at ScienceDirect

Journal of Hydrology

journal homepage: www.elsevier.com/locate/jhydrol

Research papers

High-resolution 2D shallow water modelling of dam failure floods for emergency action plans

Alessia Ferrari *, Renato Vacondio, Paolo Mignosa

Department of Engineering and Architecture, University of Parma, Parco Area delle Scienze 181/A, 43124 Parma, Italy

ARTICLE INFO

This manuscript was handled by Corrado Corradini, Editor-in-Chief, with the assistance of Valentina Ciriello, Associate Editor

Keywords:
Dam failure-induced floods
Dam-break
Dam-breach
Shallow water modelling
Hazard assessment

ABSTRACT

This paper presents a procedure based on high-resolution shallow water modelling for assessing dam-failure hypothetical scenarios that can be useful for designing emergency action plans. The capability of accurately predicting the areas flooded by these catastrophic events, both in terms of timing and magnitude, represents indeed a key task for emergency planning. The proposed procedure relies on the adoption of a parallel two-dimensional shallow water numerical model capable of both preventing large computational times and enabling the use of high-resolution meshes without introducing approximations in the set of the governing equations. Criteria for selecting the numerical model, the input data such as bathymetry, and the initial conditions are analysed in detail. The procedure is adopted to model the flooding scenarios induced by the failure of two dams in northern Italy built for irrigation and flood mitigation purposes, respectively.

1. Introduction

Dams and reservoirs have been constructed with multiple purposes (e.g. irrigation, hydropower, water supply for domestic and industrial use, navigation and flood control) and often in correlation with the socio-economic development of their respective countries (Chen et al., 2016). The ICOLD World Register of Dams counted around 58,700 dams worldwide widespread at April 2020, but this number is estimated to grow in the future e.g. as a response to the renewable energy requirements of an increasing population (Zarfl et al., 2015). Despite the benefits on society prosperity, dams might be subject to accidents causing rapid and uncontrolled water releases. In the past, several dam failures occurred due to different causes, such as foundation deficiencies (e.g. Molare in 1935 and Malpasset in 1959), overflow of the dam (e.g. Glashütte in 2002 and Niedów in 2010), earthquake (e.g. Shihgang in 1999), design errors (e.g. Gleno in 1923), and war acts (e.g. Eder in 1943). In other cases, even if the dam did not collapse, the fall of a rockslide into the lake caused huge releases of water with dramatic consequences for the downstream territories and human lives (e.g. Vajont in 1963).

A useful instrument to mitigate the risk caused by these catastrophic events relies on the capability of reliably predicting the consequences that a dam failure-induced inundation may exert on the downstream-populated areas. For this reason, many national laws prescribe to draw up Emergency Action Plans (EAPs) with the aim of minimizing damage to life and properties in case of partial or total dam failure (e.g. by implementing early warning procedures and evacuation planning, and by identifying critical infrastructures and population at risk). Meanwhile, researchers have developed numerical models capable of reconstructing historical dam failures, such as the ones of Gleno (Pilotti et al., 2011), Bouzey (Smith, 2017), St. Francis (Begnudelli and Sanders, 2007), Sella Zerbino (Petaccia et al., 2016), Niedow (Kostecki and Banasiak, 2021) and dam overtopping, such as the Vajont disaster (Vacondio et al., 2013).

Despite the modelling of historical floods generated by dam-breaks has been widely discussed in the literature (Aureli et al., 2021), the assessment of inundation maps for the redaction of EAPs still represents a challenging task, for example due to the uncertainties in the definition of the initial conditions of the reservoir and of the dam failure mechanisms, and to the complexity of the downstream topography (sometimes with very steep slopes). Within this context, dam failure-induced floods have been recently simulated by means of simplified or one-dimensional (1D) schemes (among the others, Zhou et al., 2015; Gaagai et al., 2022; Verma & Patra, 2022), also for evaluating cascade dam risk (Zhou et al., 2020), even if two-dimensional (2D) applications have been presented (among the others Azeez et al., 2020; Urzică et al., 2021; Marangoz & Anilan, 2022; Sarchani & Koutroulis, 2022).

This paper aims at presenting a procedure based on numerical

* Corresponding author.
E-mail address: alessia.ferrari@unipr.it (A. Ferrari).

https://doi.org/10.1016/j.jhydrol.2023.129192
Received 20 July 2022; Received in revised form 20 January 2023; Accepted 25 January 2023
Available online 31 January 2023

modelling for predicting flooding scenarios due to dam failures overcoming some critical points of existing approaches, which are currently adopted in different countries to assess the hydraulic hazard and/or risk related to these events. The degree of detail of national legislations about this topic is actually slightly variable, and a review of some guidelines is here carried out in order to highlight differences and similarities of the approaches mentioned there. Starting from this, the integrated procedure here proposed focuses on the adoption of 2D shallow water models capable of accurately describing the propagation of a dam-break-induced flood on real bathymetries. High-resolution Digital Terrain Models (DTMs) are required in order to account for the presence of terrain elements that may affect the flood dynamic, such as road/channel embankments and urban areas. Focusing on the flooding scenarios, the procedure assumes a failure occurring when the water level in the reservoir equals the maximum admissible one. As upstream condition, an inflow discharge hydrograph is considered when its volume is not negligible compared to the reservoir one, as often occurs dealing with small flood mitigations dam. As failure mode, the procedure assumes a sudden collapse for concrete dams and a gradual breach evolution for earthen dams. The formation of breaches along the earthen embankments of flood detention reservoirs located in lowland is also evaluated.

The assumptions related to the dam failure mechanisms and the initial hydraulic conditions of the reservoir are discussed. The proposed procedure is applied to two reservoirs in northern Italy: a concrete dam located in the mountain (Mignano dam), and a flood mitigation dam located in lowland (Parma flood mitigation dam).

The outline of the paper is as follows: the proposed procedure is presented in Sect. 2, applied to real cases in Sect. 3 and 4 and extensively discussed in Sect. 5. Finally, concluding remarks are drawn in Sect. 6 and some of the existing legislations and guidelines to cope with dam failure scenarios are described in Appendix A.

2. A procedure for modelling and mapping dam failure hazard

A possible integrated procedure for the assessment of dam failure hazard is summarized in Fig. 1. The proposed approach requires: (i) the choice of topographic data (i.e. terrain description and roughness estimation), (ii) the assumption on the dam failure mechanism and the related initial hydraulic (and eventually boundary) conditions, (iii) the numerical modelling of the flooding scenarios and (iv) the post-processing of the output data. All these key aspects are discussed in the following sections.

2.1. Topographic data

With the aim of describing the relevant terrain elements that may interact with a dam failure-induced flood, the procedure requires the adoption of high-resolution DTMs. The use of adequate topographic information is indeed one of the key elements to obtain accurate inundation maps (Casas et al., 2006; Mason et al., 2007, 2015) and both low cost high-resolution remotely sensed data (Néelz et al., 2006) and LiDAR (Light Detection And Ranging)-based DTMs (Kakoulaki et al., 2021) are nowadays accessible.

The chosen DTM has to fulfil some properties. Firstly, it has to accurately describe the reservoir area in order to avoid over- or under-predictions of the flooded areas due to over- or under-estimations of the storage water volume: e.g. the topography of the submerged zones has to be integrated (e.g. with bathymetric surveys) if the LiDAR survey is carried out when the reservoir is not completely empty.

Moreover, the DTM has to adequately include all the relevant elements that may interact with the flood propagation, such as buildings in urban areas (Schubert and Sanders, 2012), roads, channels and embankments. Filtering algorithms often manage to remove vegetation and "false" structures potentially obstructing the flow, but they are unable to reconstruct hidden small urban features (Meesuk et al., 2015). Therefore, it is important to integrate the missing small-scale urban features in the DTM, e.g. with ground-view data (Néelz et al., 2006; Meesuk et al., 2015).

Within topographic data, it is also necessary to define the roughness parameter that quantifies the flow resistance due to e.g. surface irregularities and vegetation. Calibration procedures are best suited for estimating the roughness values characterizing the river located downstream of the dam (e.g. by reconstructing the water level time series

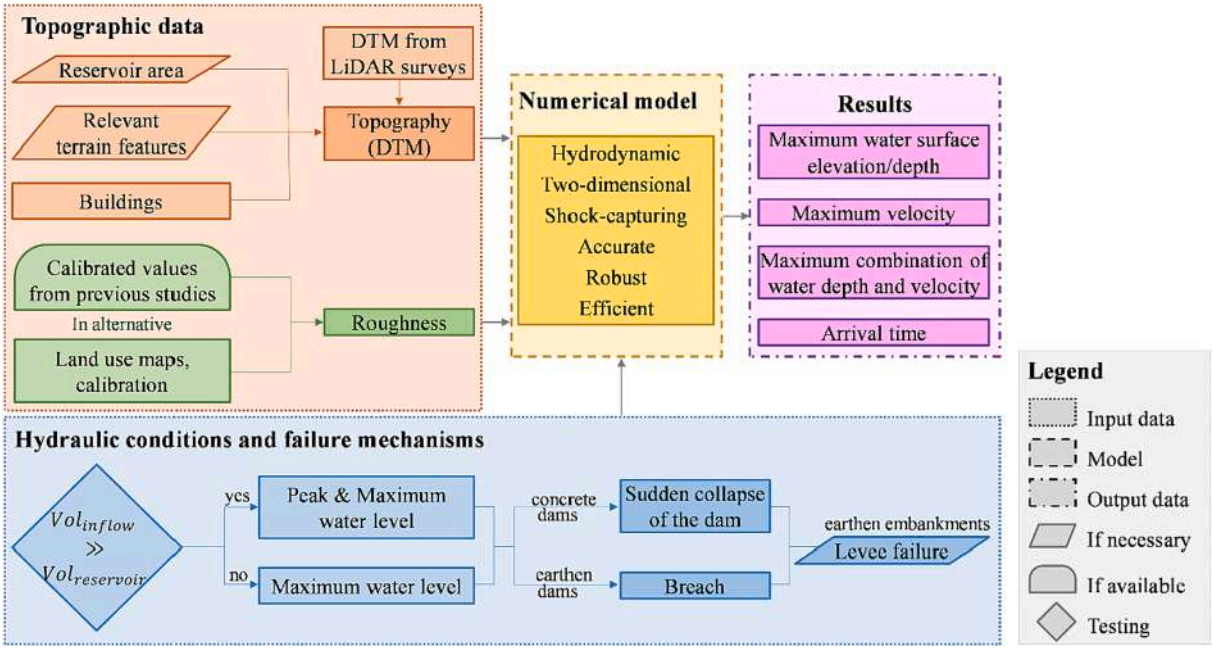

Fig. 1. Schematization of the proposed procedure for modelling and mapping dam failure scenarios.

recorded at gauging instruments). In the absence of data concerning historical flooding events, and outside of the riverbed, roughness can be inferred from literature based on land use maps.

2.2. Hydraulic conditions and failure mechanisms

The initial conditions and the failure mechanisms sketched in Fig. 1 are herein assumed (in accordance with many of the existing legislations recalled in Appendix A). With regard to the initial conditions, the methodology considers that just before the dam failure the water level in the reservoir equals the maximum admissible one, which normally corresponds to the spillway crest. An inflow discharge hydrograph (e.g. a Synthetic Design Hydrograph (SDH) with assigned return period) should be considered as upstream boundary condition when its volume is not negligible compared to the reservoir one. In this case, the maximum water level is reached at the arrival of the inflow peak; to achieve this goal, the simulation starts before the beginning of the failure in such a way that the volume of the inflow hydrograph rising limb is equal to the reservoir one at the considered water level. As a result, the peak of the inflow hydrograph superimposes the one induced by the sudden water release: this worst scenario might be quite realistic especially for relatively small flood detention reservoirs. Otherwise, if the inflow volume is negligible compared to the reservoir one, as often occurs in large mountain reservoirs with relatively small upstream watersheds, no upstream condition is imposed. For both the hydraulic conditions, the bottom outlets are assumed inoperative to increase the severity of the scenario.

As regards the failure mechanisms, the methodology assumes a sudden collapse for concrete dams and a gradual breach evolution for earthen dams (in accordance with many of the existing legislations recalled in Appendix A).

Moreover, in the presence of flood control reservoirs located in lowland, which are usually bounded by horizontal earthen embankments, the procedure assumes the formation of a breach in the levee portion that presents the higher elevation above the surrounding terrain. The breach, which is here assumed to evolve gradually, is modelled following a geometric approach and using the parameters (e.g. the final length and the evolution time) resulting from an empirical formulation (Froehlich, 2008). Based on the data collected after historical events, empirical approaches (Froehlich, 2008; Xu and Zhang, 2009; ASCE/EWRI Task Committee on Dam/Levee Breaching, 2011) define simple formulations for evaluating e.g. the formation time of the breach and its average width based on some geometric characteristics (height of the earthen dam, volume retained in the lake, etc.).

2.3. Numerical model

The numerical model used within the procedure should satisfy some requirements. Firstly, it should adopt a 2D schematization, since 1D or quasi-2D schemes, which are faster and easier to implement, are not adequate to describe flows with no predefined directions, such as dam-break-induced floods. Moreover, it should solve the complete 2D Shallow Water Equations (SWEs) in order to accurately reproduce transitions between sub- and supercritical flows and vice versa, since these phenomena, which are not rare dealing with a dam-break flow, cannot be adequately simulated by diffusive schemes (Costabile et al., 2017). With regard to the numerical approximation of the 2D-SWEs, the choice of appropriate explicit Finite Volume (FV) schemes allows reproducing, without any special treatment, transcritical flows, shock-type discontinuities, and a robust treatment of wet and dry fronts over irregular topographies (Liang and Marche, 2009). The numerical model can solve the governing equations on non-uniform meshes, either unstructured (Liang et al., 2008; Sætra et al., 2015) or structured (Vacondio et al., 2017), in order to discretize the domain with different resolution levels (thus keeping high-resolution only for relevant terrain features) and reduce the runtimes. Local time step methods may also be considered when dealing with small cells in order to avoid excessive restrictions on the time step due to the stability condition (Sanders, 2008; Dazzi et al., 2018; Hu et al., 2019a, Hu et al., 2019b). Finally, the shallow water model may also take advantage of parallelization (Sanders et al., 2010) to further reduce the computational burden: as an example, the exploitation of Graphics Processing Units (GPUs) ensured a reduction of the runtimes sometimes of two orders of magnitude with respect to CPU-based models (Castro et al., 2011; Brodtkorb et al., 2012; Vacondio et al., 2014; Lacasta et al., 2015; Juez et al., 2016; Vacondio et al., 2017).

A non-exhaustive list of 2D hydrodynamic models commonly used for flood simulations is reported in Table 1 together with their main characteristics.

2.4. Output data

Most of the measures contained in EAPs, such as the identification of the areas that can temporarily host people and the definition of roads at risk, tightly depend on the results of the numerical modelling. Therefore, the procedure suggests processing a few maps representing some useful indicators (Fig. 1), such as the maximum water depth and velocity, which enable identifying e.g. populated areas requiring evacuation, interruptions to infrastructures, erosion phenomena along overtopped embankments and stability reductions of cars and pedestrians (Milanesi et al., 2015; Arrighi et al., 2017). Water depth and velocity information can also be combined in order to assess hazard (Aureli et al., 2008; Ferrari et al., 2019; Lazzarin et al., 2022). Finally, the flood dynamic may be summarized by mapping the arrival time of the wetting front.

Beyond the contents, the output maps have to preserve a resolution similar to the one adopted in the computational grid (i.e. the high level of detail of the simulations should not be significantly downgraded by the results post-processing) and they should be provided in a format supported by GIS environment, to be used for planning operations (e.g. by overlapping other layers).

3. The case of the Mignano dam

The Mignano dam is a concrete gravity dam located in northern Italy on the Arda River, a small right tributary of the Po River (Aureli et al., 2014) (Fig. 2). At the maximum storage level, the lake created by the dam is around 2.8 km long, with an average water depth of 16.3 m (Maranzoni and Mignosa, 2019). At the elevation of the spillway crest, the maximum water depth behind the dam is around 38 m and the stored water volume is about $15 \bullet 10^6$ m^3.

The dam-break scenario was simulated using the PARFLOOD model (Vacondio et al., 2014, Vacondio et al., 2017), which satisfies the requirements outlined in Sect. 2.3. In fact, the model solves the well-balanced set of complete 2D-SWEs (Liang and Borthwick, 2009):

$$\frac{\partial \mathbf{U}}{\partial t} + \frac{\partial \mathbf{F}}{\partial x} + \frac{\partial \mathbf{G}}{\partial y} = \mathbf{S}_0 + \mathbf{S}_f \tag{1}$$

where the vectors of the conserved variables $\mathbf{U}$, and of the fluxes $\mathbf{F}$ and $\mathbf{G}$ in the x and y directions, respectively and the bed slope $\mathbf{S}_0$ and friction $\mathbf{S}_f$ source terms are defined as:

Table 1
A non-exhaustive list of 2D numerical models: governing flow equations, numerical scheme (Finite Volume, Finite Difference, Finite Elements), time discretization (Implicit, Explicit), grid type (Structured, Block Uniform Quadtree, Unstructured, Flexible), shock-capturing capability, parallel/parallelizable implementation, and website or reference paper. *Referred to the most recognised version.

Model	Equations	Scheme	Time discretization	Grid	Shock-capturing	Parallel	Website/Reference
BASEMENT	SWEs, complete	FV	I, E	U	yes	yes	https://basement.ethz.ch
FLO-2D	SWEs, complete	FD	E	S	no	no	https://flo-2d.com/
HEC-RAS	SWEs, diffusion wave approximation	FV	I	S, U	no	no	https://www.hec.usace.army.mil
InfoWorks 2D	SWEs, complete	FV	E	F	yes	no	https://www.innovyze.com/en-us/products/infoworks-icm
LISFLOOD-FP*	SWEs, local-inertial approximation	FD	E	S	no	yes	(Bates et al., 2010)
MIKE21	SWEs, complete	FV	E	F	yes	yes	https://www.mikepoweredbydhi.com/
ParBreZo	SWEs, complete	FV	E	U	yes	yes	(Sanders et al., 2010)
PARFLOOD	SWEs, complete	FV	E	BUQ	yes	yes	(Vacondio et al., 2014, 2017)
SOBEK Suite	SWEs, complete	FD	I	S	yes	no	https://www.deltares.nl/en/software/sobek/
TELEMAC 2D	SWEs, complete	FE, FV	I, E	U	yes	yes	https://www.opentelemac.org/
TUFLOW FV	SWEs, complete	FV	E	F	yes	yes	https://www.tuflow.com/

$$\mathbf{U} = \begin{bmatrix} \eta \\ uh \\ vh \end{bmatrix},$$

$$\mathbf{F} = \begin{bmatrix} uh \\ u^2h + \frac{1}{2}g\left(\eta^2 - 2\eta z\right) \\ uvh \end{bmatrix},$$

$$\mathbf{G} = \begin{bmatrix} vh \\ uvh \\ v^2h + \frac{1}{2}g\left(\eta^2 - 2\eta z\right) \end{bmatrix}, \tag{2}$$

$$\mathbf{S}_0 = \begin{bmatrix} 0 \\ -g\eta\frac{\partial z}{\partial x} \\ -g\eta\frac{\partial z}{\partial y} \end{bmatrix},$$

$$\mathbf{S}_f = \begin{bmatrix} 0 \\ -gh\frac{n_f^2 u\sqrt{u^2+v^2}}{h^{4/3}} \\ -gh\frac{n_f^2 v\sqrt{u^2+v^2}}{h^{4/3}} \end{bmatrix}$$

with h the water depth, z the bed elevation, $\eta = h + z$ the water surface elevation, u and v the velocity components along the x and y directions, respectively, g the gravitational acceleration and n_f the Manning's roughness coefficient.

The model integrates the equations through an explicit finite volume scheme and computes the numerical fluxes with the HLLC approximate Riemann solver (Toro, 2001). To avoid non-physical velocities at wet-dry fronts, the correction proposed by Kurganov and Petrova (2007) is adopted. The model achieves both first and second order of accuracy (in space and time), adopting for the latter case a depth-positive MUSCL extrapolation of the conserved variables values at the cell boundaries and a second order Runge-Kutta time integration.

The code is written in Compute Unified Device Architecture (CUDA) language, a framework introduced by NVIDIA to exploit both the GPU (the device) and the CPU (the host), ensuring speedups of two orders if compared with the CPU version. The model discretizes the computational domain with a Block Uniform Quadtree grid that allows adopting variable resolutions while preserving the GPU efficiency. For more details about the model, which was efficiently adopted also within inverse procedures (Ferrari et al., 2018), the reader can refer to Vacondio et al. (2014, 2017).

3.1. Model setup

The DTM adopted in the simulation derived from a LiDAR survey carried out upon the Arda valley in 2017: it presents a resolution of 1 m $\times$ 1 m and it covers an area of about 200 km^2. Following the items described in Sect. 2.1, the bathymetry of the lake was firstly integrated using a survey carried out in 2015 when the reservoir was empty for maintenance purposes. Then, some levee crests of the downstream reach of the Arda River, which were not adequately described in the DTM due to the presence of dense vegetation along the banks, were corrected based on a classical topographic survey. Finally, the buildings of Fiorenzuola d'Arda village were explicitly described in the computational mesh following the "building hole" method in order to reproduce local variations of the flow field (Schubert and Sanders, 2012). It is worth

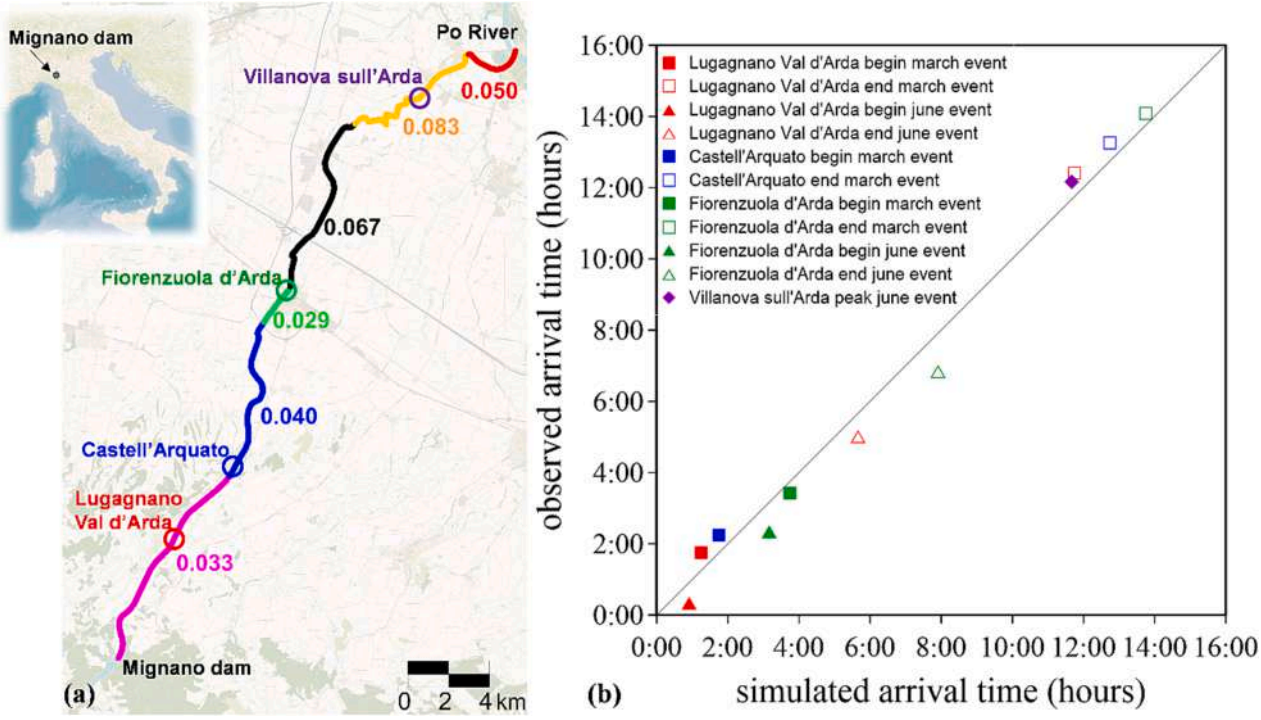

Fig. 2. (a) Manning's roughness values ($m^{-1/3}s$) assigned to the Arda River and (b) comparison between observed and simulated arrival times of March and June 2018 events. For the gauging stations up to Fiorenzuola d'Arda both begin and arrival times of the release are recognisable, whereas for Villanova sull'Arda only the peak is evident. The arrival times are normalized against the starting time of the release.

mentioning that other approaches can be adopted when simulating the effects exerted by urban areas on the flood propagation, such as the one based on the solution of the shallow water equations with porosity (e.g. Ferrari et al., 2019; Ferrari & Viero, 2020; Ayoub et al., 2022 among the others).

The domain was discretized through a BUQ multi-resolution grid (Vacondio et al., 2017): the highest resolution (2 m) was imposed in the reservoir, along the river and in urban areas, whereas road/railway embankments and rural zones were described with 4 m and 8 m, respectively. The computational grid entailed about $13.9 \bullet 10^6$ cells.

3.2. Model calibration

The roughness coefficient characterizing the river region was

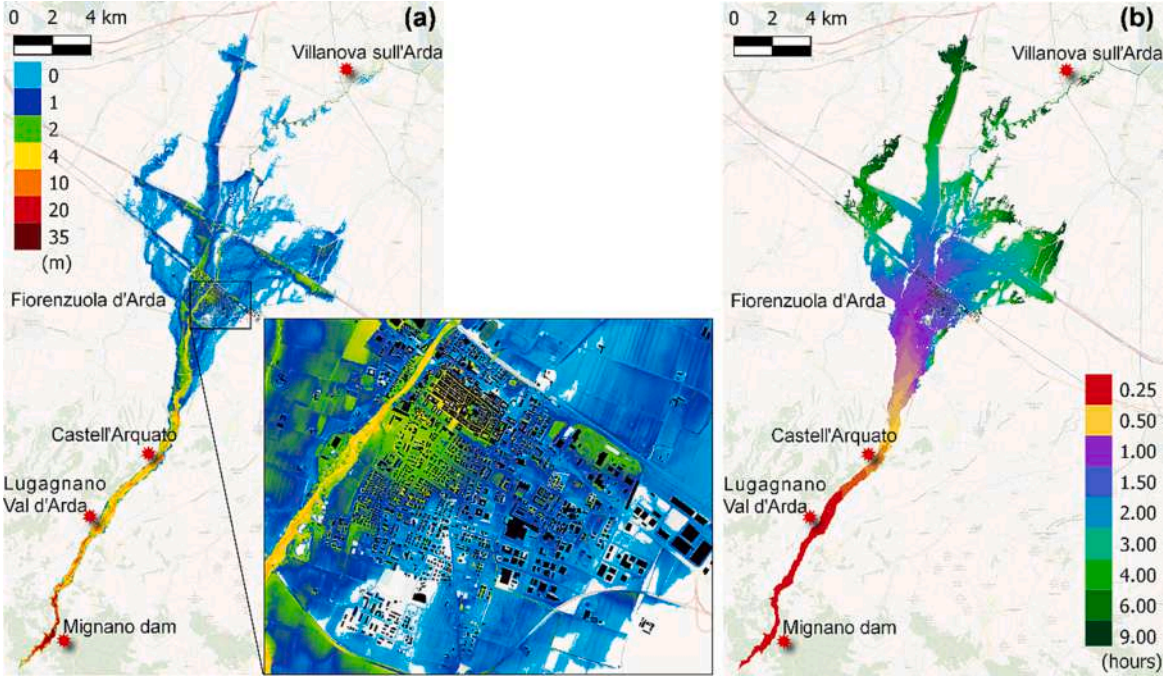

Fig. 3. Mignano dam-break: resulting (a) maximum water depths and (b) arrival times. Background map: © OpenStreetMap contributors. Buildings: https://geoportale.regione.emilia-romagna.it.

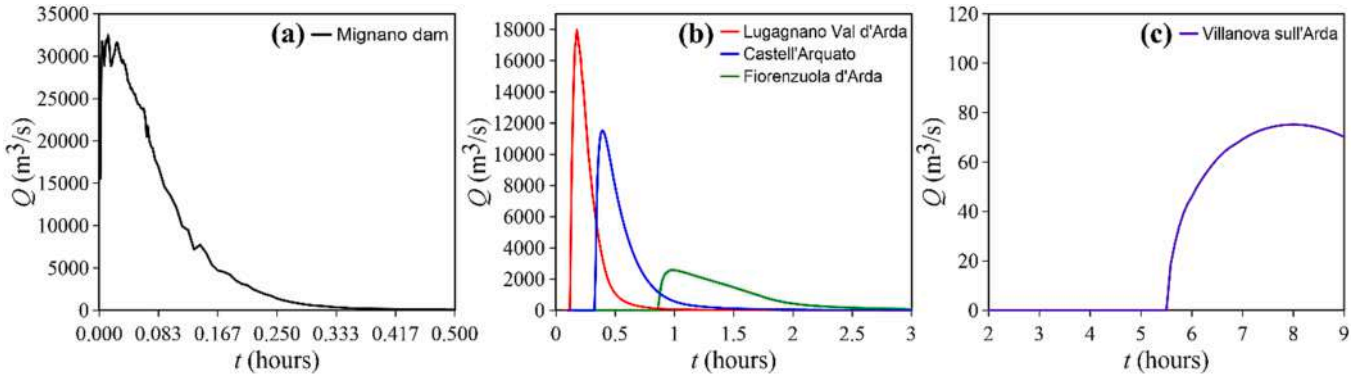

Fig. 4. Mignano dam-break: resulting discharge hydrographs at some relevant sections marked in Fig. 2.

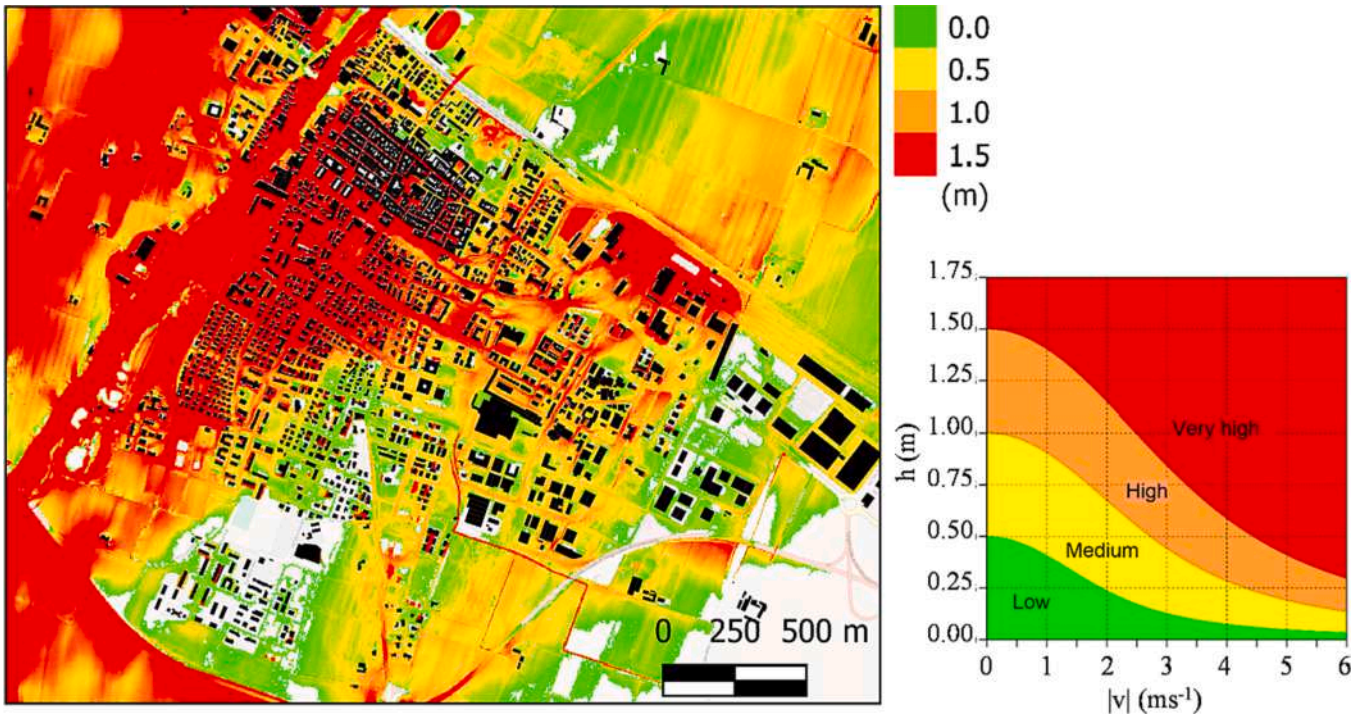

Fig. 5. Mignano dam-break: maximum total depth indicator at Fiorenzuola d'Arda village. The right panel sketches the h-|v| plane relating the maximum total depth and the hazard degree. Background map: © OpenStreetMap contributors. Buildings: https://geoportale.regione.emilia-romagna.it.

calibrated by reproducing the arrival times of some flood waves, which were artificially generated through the opening of the dam's bottom outlets, at several gauging stations (Fig. 2).

Conversely, the roughness parameter of rural areas was estimated based on literature values. By modelling the flooding time evolution of historical dam-breaks, in fact, some authors assumed coefficients in the range of 0.025–0.1 $m^{-1/3}s$ (e.g. Valiani et al., 2002; Pilotti et al., 2011; Petaccia et al., 2016). Moreover, Vacondio et al. (2016) adopted a value of 0.05 $m^{-1/3}s$ to reproduce the arrival times of a levee-breach-induced flooding occurred in a nearby river in 2014: since the area here involved presents quite similar characteristics, the same value was assumed in this work. A sensitivity analysis was however performed (see Sect. 5) in order to evaluate the influence of the roughness parameter on the water depths and arrival times of the simulated scenario.

3.3. Dam-break flooding scenario

Following the procedure described in Sect. 2.2, the instantaneous collapse of the concrete gravity dam was assumed to occur with an initial water level in the reservoir equal to the spillway crest. No inflow hydrograph was imposed, since the upstream catchment is only 70 km^2 wide and the volume of the 200-year return period SDH does not significantly over exceed the reservoir one. As downstream boundary condition, a stage-discharge relationship was imposed at the confluence between the Arda River and the Po River.

The map of the maximum (non-simultaneous) simulated water depths is shown in Fig. 3a, where the inset depicts the flooding of the Fiorenzuola d'Arda village, the most inhabited and affected one.

The peak discharge at the dam site (Fig. 4a) is around 31000 m^3/s (oscillations around the peak are due to 2D effects of water converging toward the dam section), about two orders of magnitude greater than the peak of the 200-year return period hydrological event estimated at the entrance of the lake (≈ 450 m^3/s).

In 20 min, a halved flood peak reaches the nearest village of Lugagnano Val d'Arda (Fig. 4b) potentially causing the demolition of bridges and buildings: 10 min later, the reservoir is completely emptied. Moving downstream, the Fiorenzuola d'Arda village is flooded in 1 h (Fig. 3b), whereas the northernmost areas are reached in 6 to 9 h: the peak discharge at Villanova sull'Arda is similar to the conveyable capacity of the river (Fig. 4c).

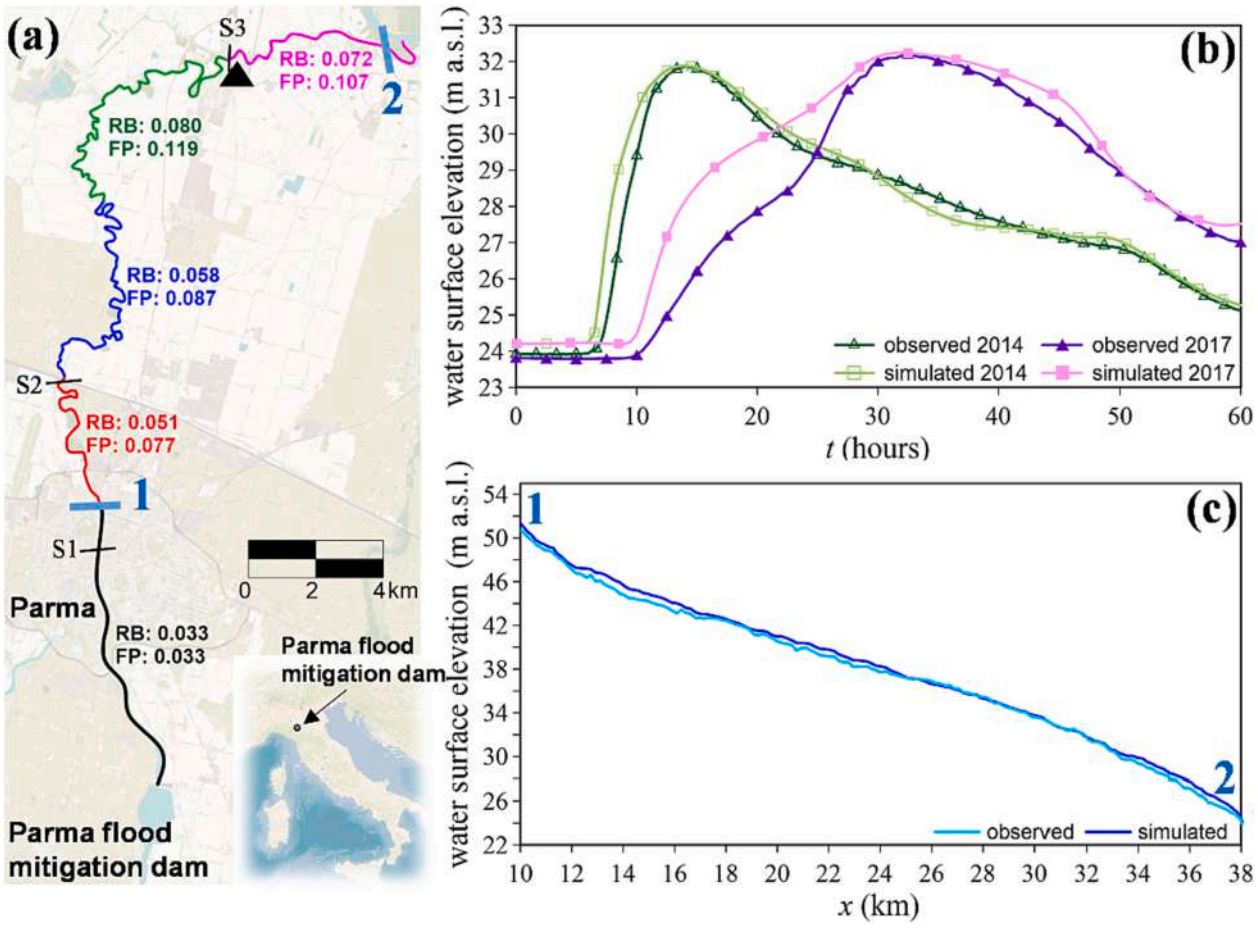

Fig. 6. (a) Manning's roughness values ($m^{-1/3}s$) assigned to the riverbed (RB) and the floodplains (FP) of the Parma River, (b) comparison between observed and simulated water level time series at the downstream gauging station of Colorno (whose location is sketched with a triangle in (a)) for two historical events and (c) comparison between observed and simulated maximum water surface elevation profile for the 2014 event (from section 1 to section 2).

With the purpose of considering the simultaneous effect of water depth and velocity for flood hazard assessment, the maximum total depth D is adopted (Aureli et al., 2008; Ferrari et al., 2019):

$$D = h\sqrt{1 + 2Fr^2} \tag{3}$$

where h represents the water depth and Fr the Froude number: values of D equal to 0.5, 1.0 and 1.5 m were assumed to bound low, medium, high and very high hazard (Fig. 5). The focus on Fiorenzuola d'Arda (Fig. 5) shows that more than half of this area presents high and very high hazard values thus highlighting the importance of defining adequate flood management strategies to avoid human life losses.

4. The case of the Parma flood mitigation dam

The Parma flood mitigation dam is located in northern Italy on the Parma River, a right tributary of the Po River (Fig. 6). The reservoir, which is bounded by earthen levees, is usually empty and used to mitigate floods potentially threating the town of Parma; the storage volume at the spillway crest level is about $10 \bullet 10^6$ m^3. When a flood wave occurs, the three movable gates at the bottom outlets of the concrete dam are progressively lowered in order to release a discharge conveyable by the river: the stored water volume is then released at the end of the event.

4.1. Model setup

The DTM adopted in the simulations presents a resolution of 1 m × 1 m and it derived from recent LiDAR surveys carried out when the reservoir was empty. The studied domain was discretized through a BUQ multi-resolution grid (Vacondio et al., 2017): the highest resolution (2 m) was imposed in the reservoir, in urban areas (buildings in the town of

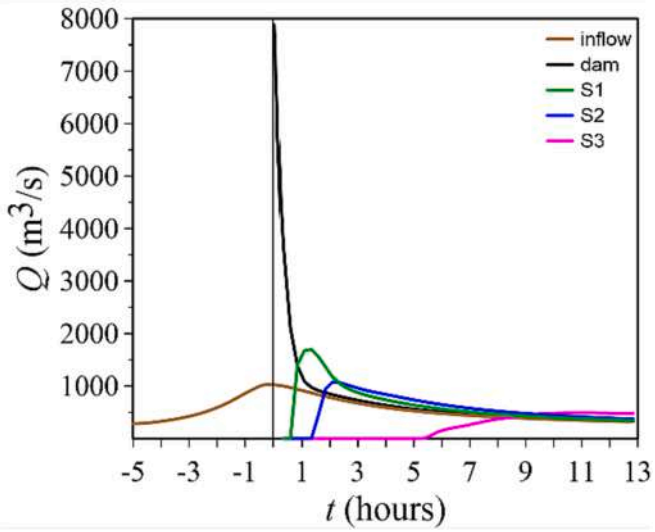

Fig. 7. Parma dam-break: resulting discharge hydrographs at some relevant sections marked in Fig. 6.

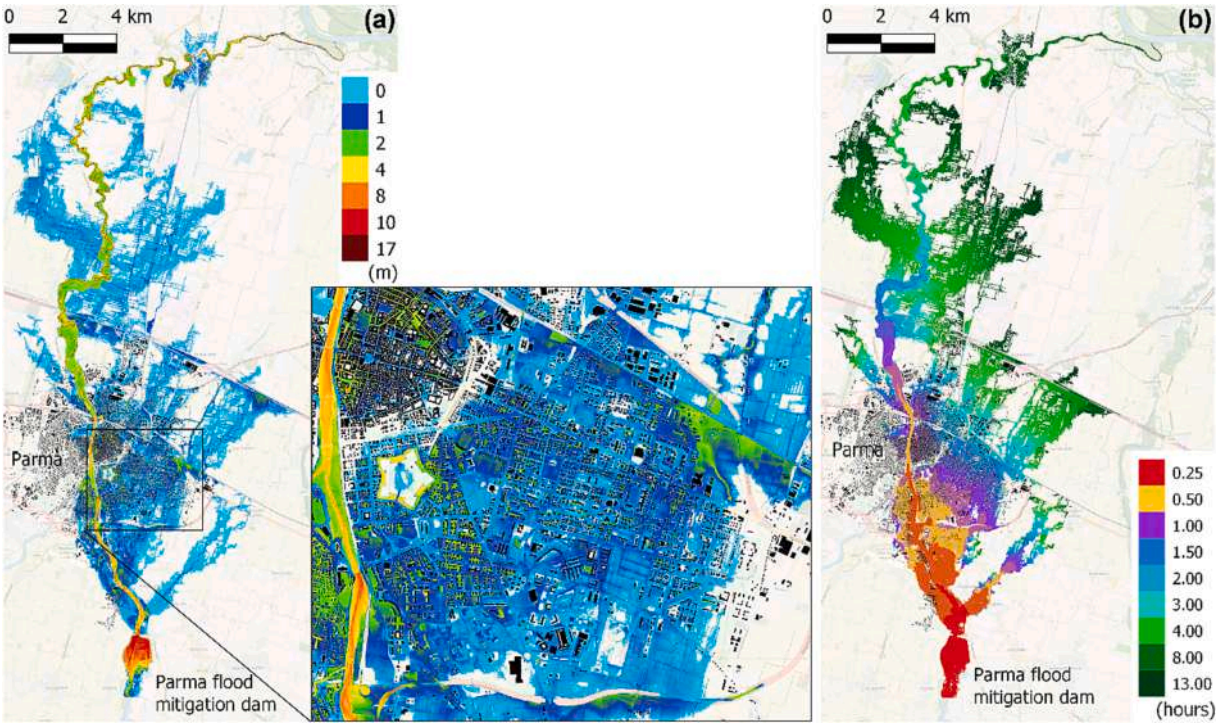

Fig. 8. Parma dam-break: resulting (a) maximum water depths and (b) arrival times. Background map: © OpenStreetMap contributors. Buildings: https://geoportale.regione.emilia-romagna.it.

Parma were modelled following the "building hole" method, Schubert and Sanders, 2012), along the river and road/channel embankments, whereas the lowest resolution (8 m) was assigned to rural zones. The computational grid entailed about $20 \bullet 10^6$ cells.

4.2. Model calibration

The river roughness was defined by reconstructing recent flood hydrographs, i.e. by reproducing the maximum water surface elevation profiles along the river and the water level time series recorded in a downstream gauging station (Fig. 6). For the floodable areas outside the riverbed, the value of 0.05 $m^{-1/3}s$ was assumed (Sect 3.2).

4.3. Dam-break flooding scenario

Following the procedure described in Sect. 2.2, the concrete gravity dam was assumed to collapse when the initial water level in the reservoir reached the spillway crest. A 200-year return period inflow hydrograph was imposed as upstream condition, since its volume ($\approx 73 \bullet 10^6$ m^3) is almost an order of magnitude greater than the reservoir one ($\approx 10 \bullet 10^6$ m^3). The bottom gates were considered closed before the failure and the reservoir was progressively filled by the incoming flood wave: when the water level in the reservoir reached the spillway crest, i.e. when the inflow peak occurred, the concrete dam was assumed to collapse.

As downstream boundary condition, a stage-discharge relationship was imposed at the confluence between the Parma and the Po Rivers (as for the Mignano scenario, the influence of this condition on the flood is substantially negligible).

The resulting flood wave at the dam site presents the same volume of the inflow hydrograph (the reservoir was initially empty), but the peak discharge is 8 times higher due to the overlapping between the hydrological peak and the dam-break-induced one (Fig. 7). The discharge hydrographs reached in sections S1 and S2 exceed both the conveyable capacity of the river and the peaks of a 200-years hydrological event. Even in section S3, although the discharge has significantly reduced, the flood is not yet completely contained in the river due to the presence of a bottleneck in correspondence of an ancient bridge.

More than half of the town of Parma is flooded in less than 1 h (Fig. 8) reaching medium–high velocity values and high-very high hazard (total depth) ones (Fig. 9), whereas the northernmost lowland areas are flooded in 5 to 10 h.

4.4. Dam-breach flooding scenarios

Since the Parma flood mitigation dam presents earthen embankments, flooding scenarios induced by the formation of breaches were also simulated (Sect. 2.2) by assuming a 1000-year SDH entering the reservoir, closed dam bottom gates and clogged spillway. This latter assumption was introduced since wooden debris carried by the incoming flood might partially (or totally) hit the piers located along the spillway crest to support roads (e.g. the Palagnedra dam overtopping case, Bruschin et al., 1982). The breach was assumed to develop when the water level in the reservoir reached the levee crest elevation simultaneously with the inflow peak. As the levee crest is horizontal, two breach locations were independently simulated in the northernmost portion of the levee close to the dam (on the right and on the left side, respectively), where the embankments reach the maximum elevation of around 12 m above the surrounding terrain (Fig. 10). The breaches were modelled with a geometric approach (Ferrari et al., 2020) adopting the Froehlich formula (Froehlich, 2008):

$$\overline{B} = 0.27 K_0 V_W^{0.32} H_b^{0.04} \tag{4}$$

$$t_f = 63.2 \sqrt{\frac{V_W}{g H_b^2}} \tag{5}$$

where $\overline{B}$ represents the final average width (side slope 1:1 is assumed for overtopping failures), K_0 is a factor accounting for the failure mode (e.g. $K_0 = 1.3$ for overtopping), V_W denotes the water volume above the breach bottom at the beginning of the failure, H_b is the final height of the breach and t_f the breach formation time.

The breach reached a final averaged width of 78 m in 2.1 h. Slightly

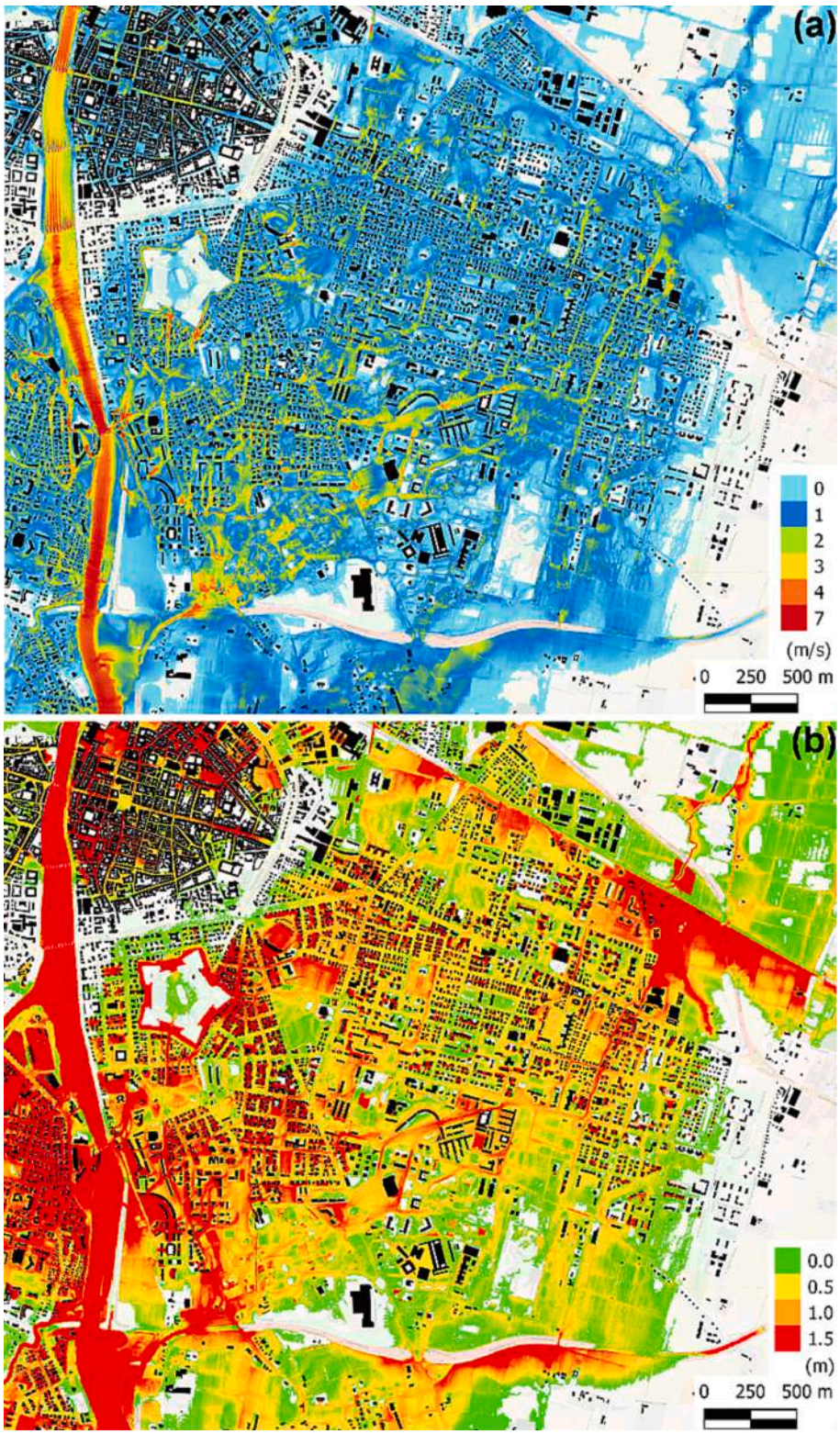

Fig. 9. Parma dam-break: maximum (a) velocities and (b) total depths reached in the town of Parma. Background map: © OpenStreetMap contributors. Buildings: https://geoportale.regione.emilia-romagna.it.

different values result by adopting other empirical formulas, such as the one proposed in Xu and Zhang (2009): in this case, the breach would open in about 2.8 h reaching the maximum width of 63 m.

The maps of the maximum water depths resulting from the left and right breach openings, which are shown in Fig. 10, highlight the macroscopic difference between the two flooding scenarios. At the occurrence of the left levee failure, the discharge flowing through the breach partially propagates west of the Parma River and partially flows back into the unleeved riverbed just downstream the dam. Even if the outflow peak discharge (Fig. 11) is less than half of that caused by the instantaneous collapse of the dam (Fig. 7), both the Parma downtown and lowlands are flooded. Conversely, the wave flowing out from the

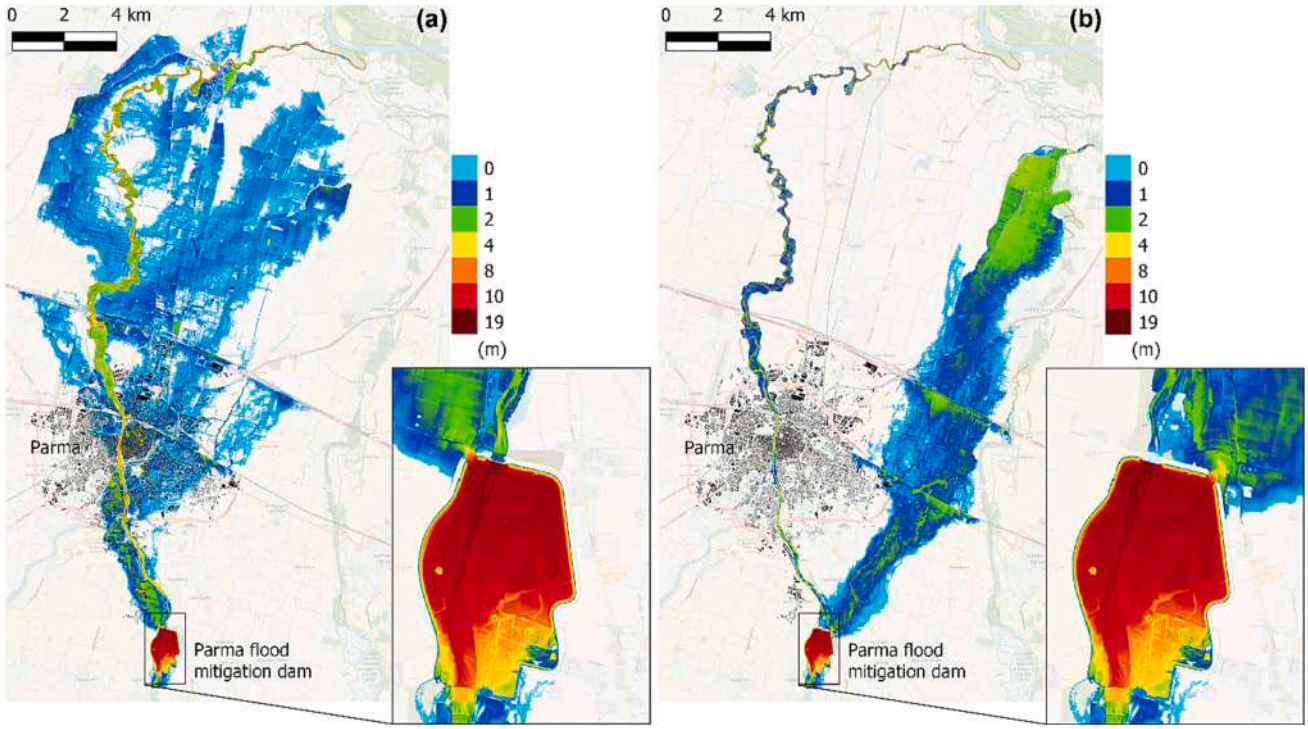

Fig. 10. Parma dam-breaches: maximum water depths resulting from (a) the left and (b) the right breach openings. Background map: © OpenStreetMap contributors. Buildings: https://geoportale.regione.emilia-romagna.it.

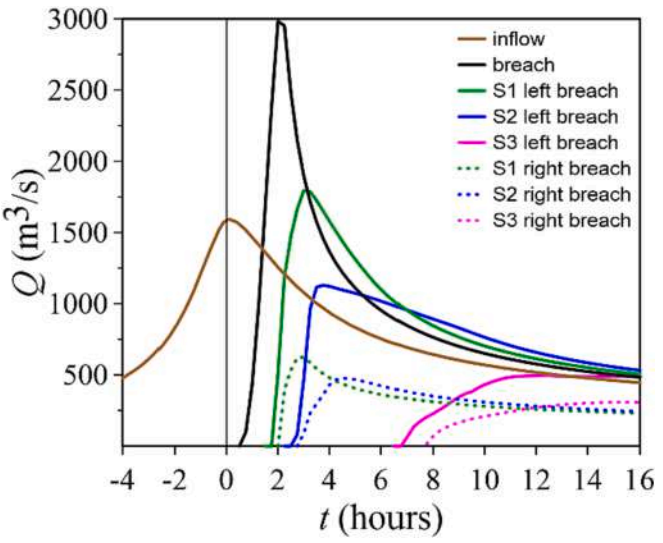

Fig. 11. Parma dam-breaches: resulting discharge hydrographs from the left and the right breach openings at some relevant sections marked in Fig. 6.

right breach mostly propagates northeast, probably in an ancient paleochannel of the Parma River, and only a small part flows back into the current riverbed (Fig. 10b); in this scenario, the Parma downtown is preserved from flooding, but other small villages in lowlands at east are instead heavily involved.

5. Discussion

In this section, the main assumptions of the proposed procedure are critically analysed regarding recent literature in order to outline the reliability of the results. Model topography was derived by selectively downsampling a high-resolution 1 m × 1 m DTM (obtained from a LiDAR scan) in such a way that the main characteristics influencing the flooding dynamics are kept unchanged. Uncertainty may rely on the roughness values assumed for the floodable areas, since the discharge conveyed in the river is a small fraction of the one caused by the failure. A sensitivity analysis was then performed for the Mignano case by considering roughness variations in the range of ± 25%. The resulting flooded areas are compared in Fig. 12 for the northernmost part of the domain, where the wetting front fragments on lowlands and roughness plays a more relevant role. Given a total flooded area of 69 km^2 resulting from the reference simulation, the adoption of 25% higher and lower roughness values determines the flooding of around 67 and 70 km^2, respectively (the differences are less than 3%). Even the arrival times show moderate variations, which cannot substantially affect the planning of safety interventions.

The adoption of a 2D shallow water model has proved to be fundamental for modelling the impacts of dam failures, since the flooding dynamic of these events cannot be defined a priori, e.g. when paleochannels are reactivated during the flood propagation (Fig. 10b). Even the shallow water approximations may in some cases do not strictly hold, e.g. near the dam soon after the collapse, but despite some studies overcame this issue solving for example Vertically Averaged and Moment (VAM) equations (Cantero-Chinchilla et al., 2020) or fully 3D equations through Lagrangian approaches (e.g. Smoothed Particle Hydrodynamics, Vacondio et al., 2013), their use in real cases is still limited by the high computational burden.

The adopted numerical model solves the complete 2D-SWEs since diffusive schemes, which neglect inertial terms, are not suitable for modelling these rapidly varying flows, mainly due to their inability to manage the transitions between sub- and supercritical flows and vice versa, and to the fact that inertial terms play an important role (Mignosa et al., 2018; Costabile et al., 2020, 2017; Dazzi et al., 2021). In order to better clarify this latter issue, the momentum equations of the SWEs are written in 2D non-conservative form:

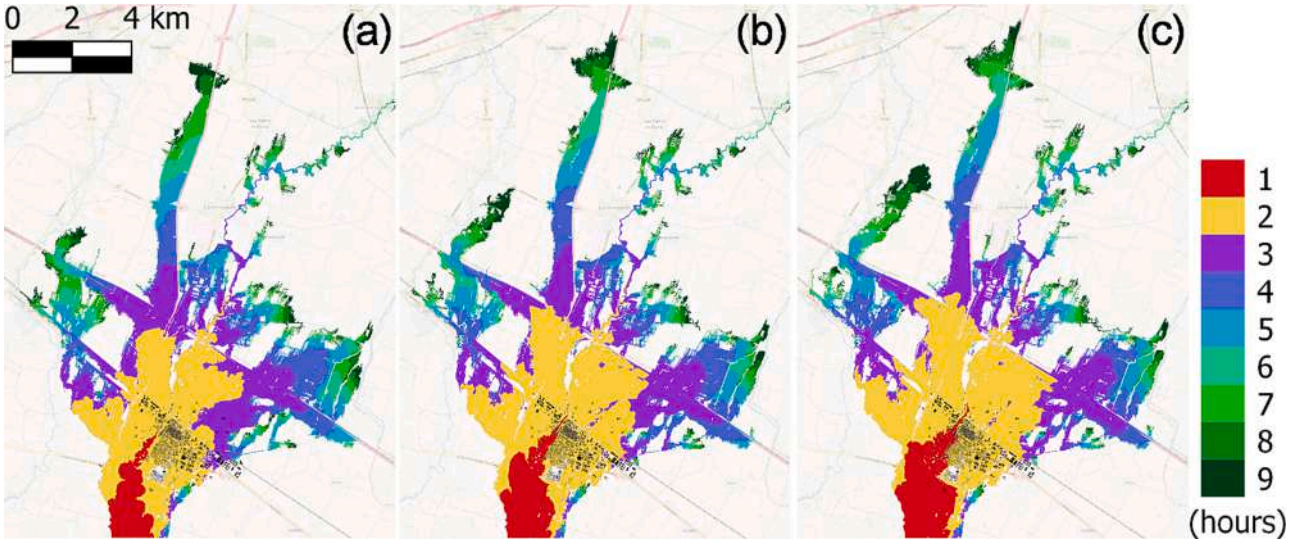

Fig. 12. Mignano dam-break. Details of the arrival times resulting by adopting (a) a 25% increase of the reference roughness values, (b) the reference values and (c) a 25% decrease of the reference values.

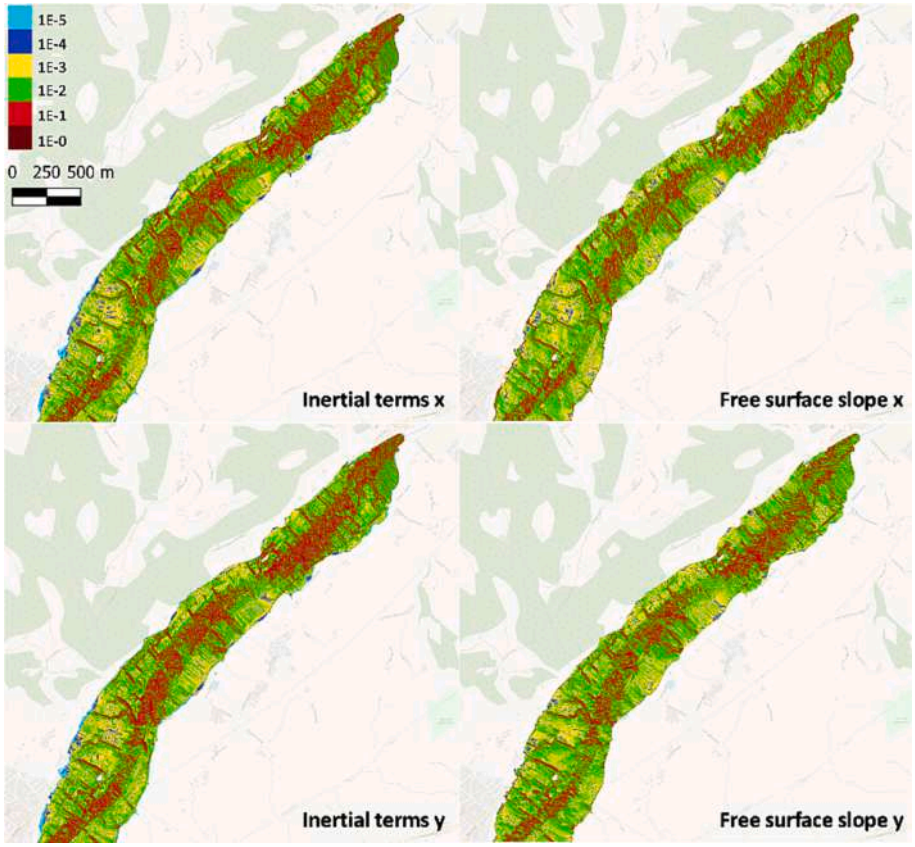

Fig. 13. Mignano dam-break. Arrival of the flood wave at Lugagnano Val d'Arda village: inertial terms and free surface slope resulting along the *x* and y direction.

$$\begin{cases} \frac{1}{g}\frac{\partial u}{\partial t} + \left[\frac{u}{g}\frac{\partial u}{\partial x} + \frac{v}{g}\frac{\partial u}{\partial y} + \frac{u}{g}\frac{\partial v}{\partial y}\right] + \frac{\partial \eta}{\partial x} + S_{fx} = 0 \\ \frac{1}{g}\frac{\partial v}{\partial t} + \left[\frac{v}{g}\frac{\partial u}{\partial x} + \frac{u}{g}\frac{\partial v}{\partial x} + \frac{v}{g}\frac{\partial v}{\partial y}\right] + \frac{\partial \eta}{\partial y} + S_{fy} = 0 \end{cases} \quad (6)$$

where the first term denotes the local acceleration slope, the second one (the whole square brackets) the convective acceleration slopes, the third one the water surface slope and the last one the friction slope.

As shown in Fig. 13 for a selected time after the Mignano dam-break, the values of the inertial terms (sum of the local and the convective acceleration slopes) are of the same order of magnitude of the water surface slope: neglecting these terms would thus lead to unacceptable approximations in the numerical results.

A high return period SDH (T = 200 or T = 1000 years) was imposed as upstream boundary condition in the case of the Parma flood mitigation dam, since its volume was significant with respect to the reservoir one. Moreover, the dam/levee failure was assumed to occur at the

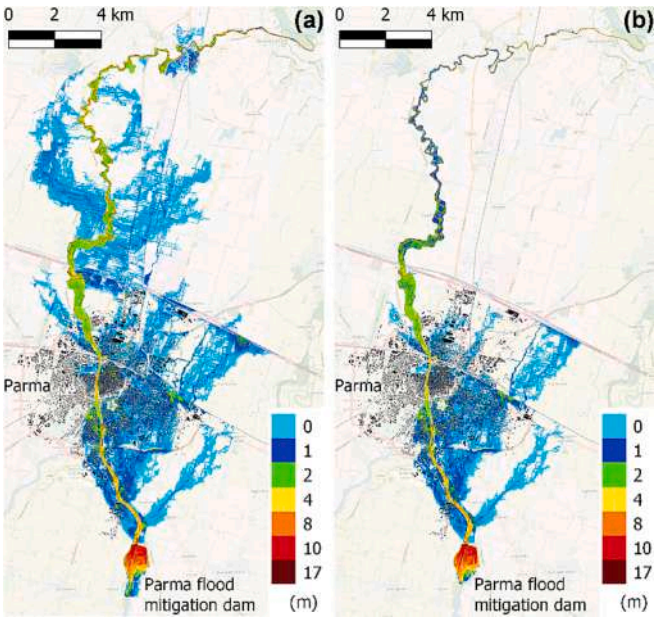

Fig. 14. Parma dam-break (a) with and (b) without an inflow hydrograph: maximum water depths. Background map: © OpenStreetMap contributors. Buildings: https://geoportale.regione.emilia-romagna.it.

arrival of the inflow peak, since dealing with a flood control reservoir that is usually empty, the failure is expected to be correlated with a flood event: as shown in Fig. 14 for the dam-break scenario, the absence of an inflow hydrograph would largely underestimate the downstream-flooded areas.

With reference to the failure mode, concrete dams were assumed to collapse also considering that similar events were already experienced in the past (e.g. Malpasset dam, Valiani et al., 2002). As regards the modelling of embankment breaches, coupled hydrodynamic-erosion models inherently account for both the hydrodynamic conditions and the levee characteristics. However, they require the knowledge of some parameters characterizing the levee material, such as the porosity p, the critical shear stress τ_c and the erodibility coefficient k_d: even if the first one can be easily assessed with local surveys and the others retrieved in the literature, there is still some uncertainty in the values to be adopted. Since during a breach evolution the effective shear stresses τ are usually-one or, more frequently, two orders of magnitude higher than the critical ones, a sensitivity analysis was here carried out with reference to the erodibility parameter, by adopting a physically-based approach that couples the 2D-SWEs with an erosion model (Dazzi et al., 2019):

$$\frac{\partial z(x,y)}{\partial t} = -\frac{k_d \max(\tau - \tau_c; 0)}{1-p} \tag{7}$$

In the analysis, three values of the erodibility coefficient were tested: the one calibrated in Dazzi et al. (2019) to simulate a real breach occurred in a nearby river (k_{d_2}), a 50% lower value (k_{d_1}) and a 25% higher one (k_{d_3}). As shown in Fig. 15, the breaches resulting by adopting the geometric approach and the erosion model are quite similar: the latter ones evolve in 2 to 3 h reaching average widths from 70 to 105 m, and the outflow hydrographs, although presenting different shapes have quite similar peak values. The peak discharge resulting from the geometric model is about 30% higher than that obtained with the erosion model: this causes the heaviest effects, at least near the breach, whereas far away, the differences progressively reduce, but this aspect deserves further investigation.

Finally, other physical phenomena that might locally influence the propagation of the dam failure-induced floods are: the potential collapse of buildings or infrastructures, the transport of solid material (rocks, wooden debris, remnants of buildings and of the dam itself) and soil erosion. For the two considered test cases, these phenomena were considered negligible. The collapse of buildings and infrastructures might affect only the narrow valley downstream the Mignano dam, where the flood wave still has enough energy to destroy buildings, whereas elsewhere (and for the Parma mitigation dam), only bridges in the river, which are almost all overtopped by the flow, may be damaged. This aspect might be considered when modelling dams with large reservoirs located in valleys with steeper slopes (e.g. Milanesi and Pilotti, 2021). As regards solid material, which in some cases may play a relevant role, recent studies investigated the blockage of reservoir spillways

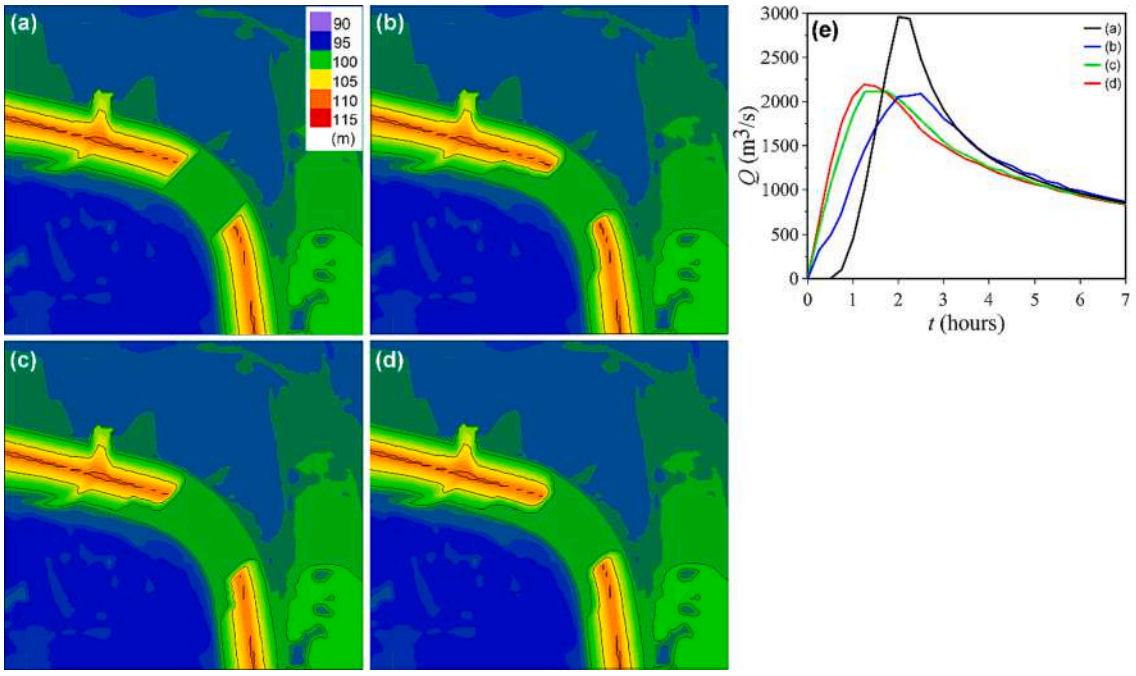

Fig. 15. Parma dam-breach: bottom elevation near the right levee breach obtained with (a) the geometric approach and an erosion model with (b) k_{d_1} < (c) k_{d_2} < (d) k_{d_3}, and (e) hydrographs resulting through the breach.

Table A1
Highlights of the analysed legislations.

	Norms	Initial conditions of the reservoir and failure mechanism	Numerical model	Results
Italy	2014, Directive "*Indirizzi operativi inerenti l'attività di protezione civile nell'ambito dei bacini in cui siano presenti grandi dighe*". 1995, Circular letter DSTN/2/22806	Concrete dams: water level at the spillway crest and total/partial collapse of the dam. Earthen dams: water level at the crest elevation (due to a severe flood wave entering the reservoir) and partial breach failure.	Validated numerical model.	Map of floodable areas. Tables concerning the principal variables of interest.
Switzerland	2012, OSOA 721.101.1 2015, "*Directive sur les ouvrages d'accumulation*", part E	Water level equal to the corresponding level for determining the dam. The break mechanism depends on the dam structure.	1D, 2D models. The flood wave may be estimated using also simplified procedures.	Map of the arrival times.Water depth and velocity resulting in each cross section (1D models) or in selected cells (2D models). Shape files of the water depth and velocity head maps.
England	*Flood and Water Management Act 2010* *Reservoirs Act 1975* *Guidance for drawing reservoir flood maps* *Guide to risk assessment for reservoir safety management*	Two main scenarios are: 1. Water level at the spillway level and normal water level in the river; 2. Water level higher than the top water level and extreme natural flood on the downstream river.	Rigorous 2D flow models capable of simulating extreme and rapidly varying flows for the quantitative risk assessment.	Maps of the maximum water depth and velocity.
Finland	*Dam Safety Act* (DSA) 494/2009 *Government Decree on Dam Safety* (DDS) (319/2010) 2018, *Dam Safety Guide* (DSG)	Depending on the dam structure and its resistance to erosion, and considering both normal and flood situations.	1D or 2D dynamic flow equations for the modelling of channel flows.	Map of the maximum flood coverage, flood evolution, maximum water depth, arrival times of the wetting front and of the maximum water level at each cross-section. For 2D models: maximum flow velocity and a damage parameter. Summary tables with the values of these variables of interest.
USA	1979, *Federal Guidelines for Dam Safety* 2013, *The Federal Guidelines for Inundation Mapping of Flood Risks Associated with Dam Incidents and Failures*	Two main scenarios are: 1. Hydrological breaches occurring with extreme precipitation and runoff; 2. "Sunny day" breaches occurring during fair weather without an inflow.	Simplified methods, 1D and 2D models.	Inundation maps whose features are defined to properly fit the end use (e.g. emergency response and mitigation planning).
India	2018, "*Guidelines for Mapping Flood Risks Associated with Dams*"	Fair weather and hydrological failure event depending on the hazard classification of the dam and population at risk.	Simplified methods, 1D and 2D models.	Maps of maximum water depth, velocity and inundation duration.

due to large wood (Furlan et al., 2021) and the transport of floating wooden material in rivers (Persi et al., 2022), but their extension to dam-break-induced floods is still challenging. Focusing on the bed erosion/deposition mechanisms, which are often studied through laboratory investigations (e.g. Khosravi et al., 2021), despite some 2D models adopting different sediment transport formulations well reproduced laboratory experimental data (among the others Xia et al., 2010; Soares-Frazão et al., 2012), their application to prototype scale on complex topographies and with huge discharges deserve further investigation.

6. Conclusions and future work

Floods induced by dam failures are by far less frequent than that generated by hydrological events, but their catastrophic consequences require an enhancement of the management strategies. With the aim of improving hazard mapping, this paper proposed a procedure based on shallow water modelling. The application of the procedure to two reservoirs in northern Italy characterized by different purposes, volume and location allowed assessing the following items:

- The flooding scenarios have to be simulated using a fully 2D shallow water model, since inertial contributions play a relevant role (in the Mignano case, inertial terms and water surface slope have the same order of magnitude), and no preferential flow directions can be assumed a priori (in the Parma test, an ancient paleochannel in rural areas was reactivated);
- The flooding dynamic is only marginally influenced by the roughness coefficient used to describe the rural areas: the sensitivity analysis on the Mignano dam case highlighted only moderate variations of the flooded areas and of the arrival times;
- An inflow discharge hydrograph has to be imposed as upstream condition, e.g. when dealing with flood mitigation dams, which are usually empty before a flood wave occurs. The results for the Parma flood mitigation dam, which unlike the Mignano dam is usually empty and with a non-negligible inflow hydrograph, confirmed the importance of considering an inflow condition;
- Multiple breach locations should be considered when dealing with reservoirs bounded by horizontal earthen embankments. The modelling of two bank failures along the embankments of the Parma reservoir, one at the left and one at right of the dam, was fundamental to capture flooded areas far from the dam that otherwise would erroneously be considered safe;

The procedure can be extended to other similar dams when dealing with emergency planning.

The dynamic modelling of building collapse due to flood impact is left to future work.

CRediT authorship contribution statement

Alessia Ferrari: Methodology, Software, Validation, Formal analysis, Writing – original draft. **Renato Vacondio:** Supervision, Conceptualization, Methodology, Formal analysis, Writing – review & editing. **Paolo Mignosa:** Supervision, Conceptualization, Methodology, Formal analysis, Writing – review & editing.

Declaration of Competing Interest

The authors declare that they have no known competing financial interests or personal relationships that could have appeared to influence the work reported in this paper.

Data availability

Data will be made available on request.

Acknowledgments

This work was partially funded under the National Recovery and Resilience Plan (NRRP), Mission 04 Component 2 Investment 1.5 – NextGenerationEU, Call for tender n. 3277 dated 30/12/2021, Award Number: 0001052 dated 23/06/2022. The authors gratefully acknowledge the support of CINECA under the projects STRAUSS: HP10C5OC10 and SCHUBERT: HP10CP2YN9. This research benefits from the HPC (High Performance Computing) facility of the University of Parma, Italy. The Interregional Agency for the Po River (Agenzia Interregionale per il fiume Po) and the Consorzio di Bonifica di Piacenza are gratefully acknowledged. The authors are grateful to Dr S. Dazzi for providing the erosion model and for fruitful comments. The editor, the associate editor and the reviewers are also kindly acknowledged for their valuable suggestions on the early version of the manuscript.

Appendix A. Dam failure legislations

Several countries issued laws, decrees, circular letters and guidelines to regulate some of the assumptions to be used when modelling flooding scenarios induced by dam failures, also within the framework of EAPs. In what follows, the relevant parts of these legislations are described with reference to some countries in Europe (Italy, Switzerland, England and Finland), North America (USA) and Asia (India) (Table A.1.).

A.1. Italy

The directive "*Indirizzi operativi inerenti l'attività di protezione civile nell'ambito dei bacini in cui siano presenti grandi dighe*" (promulgated in 2014) provides instructions for the management of emergency situations, e.g. by demanding flood propagation studies for the redaction of EAPs for large dams. Details regarding these studies, which have to define the areas flooded by a dam collapse or the full opening of the dam outlets, are contained in the Circular letter n° DSTN/2/22806 of 1995 "*Disposizioni attuative ed integrative in materia di dighe*". These dispositions prescribe that a dam-break scenario has to evaluate the consequences of the worst failure mechanism among those suggested for the different dam types, and that the initial conditions depend on the dam structure. As an example, the collapse of concrete dams is assumed to be sudden and complete (apart some special cases) with the water level in the reservoir at the spillway crest, neglecting both the upstream inflow and the outflow at the bottom outlets, and considering the river downstream of the dam in dry conditions. As regards the flood propagation modelling, the adoption of a numerical model that has been previously validated against real cases is prescribed. Despite no remarks regarding the choice of 1D or 2D models are explicitly provided, the result representation strictly refers to a 1D approach: beyond the redaction of an inundation map representing the floodable areas, indeed, information regarding e.g. the maximum water depth, velocity, total head, and arrival time of the flood peak has to be provided for the river reach. In addition, tables concerning the principal variables of interest are demanded.

A.2. Switzerland

The "*Ordonnance Sur les Ouvrages d'Accumulation*" (OSOA 721.101.1, 2012) provides dispositions concerning the safety of water storage structures (https://www.fedlex.admin.ch), and with regard to emergency plans, it specifies that inundation maps have to represent the zones potentially flooded in case of sudden collapse of water retaining structures. Flooding arrival times are also required to properly alert the population in case of a total and instantaneous failure: the activation of sirens is indeed required for people living in areas that would be flooded in less than two hours, whereas a general alarm system invites the population living in far areas to listen the evacuation instructions (ICOLD, 2020).

More details regarding dam-break analyses can be found in the 2015 "*Directive sur les ouvrages d'accumulation*" (https://www.bfe.admin.ch), whose part E focuses on the redaction of emergency plans. As regards the initial conditions of the dam-break scenario, the water level in the reservoir "*should be equivalent to the corresponding level for determining the height of the dam*", while different break mechanisms can be considered depending on the dam structure (e.g. the sudden break for gravity and arch dams) and in the presence of dams in series.

With respect to the result disclosure, water depth and velocity resulting in each cross section for 1D models, or in selected cells for 2D models, have to be provided; shape files of the water depth and velocity head maps are also required for the load in a GIS framework.

A.3. England

As amended by the Flood and Water Management Act 2010, the Reservoirs Act 1975 regulates reservoirs. In this framework, detailed flood maps are used by the Environment Agency to assess the reservoir risk, as well as by local authorities to prepare emergency plans in order to mitigate the effects of flooding resulting from any reservoir water escape (ICOLD, 2020).

According to the guidance for drawing reservoir flood maps (https://www.gov.uk/guidance/reservoir-flood-maps-when-and-how-to-use-them#preparing-a-flood-risk-assessment), each map actually accounts for two flooding scenarios induced by the dam/reservoir failure. The first scenario ("dry-day") assumes as initial conditions a water level in the reservoir corresponding to the spillway level and a normal level in the rivers reaches upstream and downstream of the reservoir. Conversely, the second scenario ("wet-day") assumes that just before the failure the water level in the reservoir is higher than the top water level and that the river downstream of the reservoir is already experiencing an extreme natural flood (with an annual probability of 0.1%, ADEPT-Environment Agency, 2019). As regards the failure mechanism, both scenarios assume a void occurring from the top to the base of the dam (e.g. the bed of the watercourse just downstream). Moreover, the "*Guide to risk assessment for reservoir safety management*" (provided by the Environment Agency, 2013), outlines a procedure for dams in England and Wales consisting in three principal steps (i.e. identification, analysis and evaluation of the risk) and based on three tiers that allow assessing the risk at (i) qualitative, (ii) simplified quantitative and (iii) detailed quantitative manner. As regards the modelling tool, the third tier (iii) points out that only rigorous 2D flow models are capable of simulating extreme and rapidly varying flows.

A.4. Finland

With the aim of reducing the hazard related to dams, the Dam Safety Act (DSA) 494/2009 (https://www.finlex.fi/en/laki/kaannokset/2009/en20090494.pdf) and the Government Decree on Dam Safety (DDS) (319/2010) (https://www.finlex.fi/en/laki/kaannokset/2010/en20100319.pdf) contain provisions concerning dam-break hazard analyses (ICOLD, 2020). Details about the contents of these norms and general guidelines to assess the impacts of dam breaches are also outlined in the Dam Safety Guide (DSG) (https://www.environment.fi/en-US/Waters/Use_of_water_resources/Dams_and_dam_safety/Dam_Safety_Guide), whose publication was updated in 2018. The DSG affirms that the

hazard analysis should compare different possible dam breach scenarios, depending on the dam structure and its resistance to erosion, and considering both normal and flood conditions: for example, the sudden collapse of an embankment dam is assumed to occur both due to internal erosion and overflow.

With regard to the computational model, the DSG specifies that extensive data computations are not always necessary to define the flood hazard of a dam failure. However, for the modelling of channel flows, one- or two-dimensional dynamic flow equations shall be used. As regards the resulting scenarios, the guidelines affirm that they shall be represented using maps at a convenient scale and tables. The maps should draw the maximum flood coverage, the flood evolution at relevant times (e.g. 0.5, 1, 2 and 3 h after the breach occurs), the maximum water depth, the location of the computed cross-sections, the arrival times of the wetting front and of the maximum water level at each cross-section. When dealing with 2D models, additional maps concerning the maximum flow velocity and a damage parameter (product of water depth and velocity) are required. The values of these variables of interest reached in each cross-section should also be listed in summary tables.

A.5. USA

Federal Guidelines for Dam Safety were introduced in 1979 in order to address issues concerning, among the others, dam safety, dam failure studies and inundation mapping. The Federal Guidelines for Inundation Mapping of Flood Risks Associated with Dam Incidents and Failures (FEMA, 2013) provide operational instructions to model and represent a dam breach, i.e. an opening through the dam usually associated with its total or partial failure that causes the sudden, rapid and uncontrolled empting of the reservoir.

Focusing on the hydrological conditions, two types of breaches are identified: hydrological breaches occurring with extreme precipitation and runoff, and "sunny day" breaches, which are originated during fair weather in the absence of an inflow due to storm events. If the flow generated by the dam breach is at least two times larger than the base flow, the latter can be neglected. As regards the initial water level in the reservoir, different values may be considered for the fair weather failure, e.g. normal pool elevation (usually recommended as the default volume), invert of auxiliary spillway and top of the dam. The guidelines also provide criteria for the definition of the downstream extent of the scenario. For the "sunny day" failures, the limit should be established so that the flood breach does not pose a risk to life and properties (e.g. no more habitable structures are involved, or the flow is contained in the downstream channel). Conversely, the downstream limit of hydrological failures is located where the rise in the water level is negligible, or the difference between the water surface elevations resulting from the basin runoff in the absence and in the presence of a dam failure is below a given threshold.

The breach parameters have to be selected according to some characteristics of the dam, such as the dimension, the type, the materials of construction, and the historical records (e.g. foundation problems) and a sensitivity analysis should be performed. For example, the average width of earth-fill dam breaches is 0.5–5 times the dam height, the side slope is between 0:1 and 1:1 and the formation time is between 0.1 and 4 h.

Recommendations concerning the choice of the routing model (e.g. simplified methods, 1D and 2D models) with reference to the hazard potential are also provided. The selection of the computational model, indeed, depends on the damage potentially caused by the failure according to a balanced tiered approach: for example, a tier level 3, which is applicable to a high-hazard potential due to the presence of large dams and sufficient population at risk, requires unsteady-one-dimensional models or two-dimensional ones for the downstream routing of the breach hydrograph. To properly fit the end use (e.g. emergency response and mitigation planning) the features of the inundation maps are finally described: the adoption of base maps (e.g. orthophotographic or planimetric) over which representing the inundation information and the delineation of inundation polygons are some of the recommended elements to provide easy-to-use hardcopy inundation maps.

A.6. India

Under the Dam Rehabilitation and Improvement Project, the Government of India established in 2018 "*Guidelines for Mapping Flood Risks Associated with Dams*" (Central Water Commission, 2018) in order to facilitate the preparation of emergency action plans for dams. Focusing on the redaction of inundation maps, the guidelines analyse the types of possible dam failures and summarize the formulas and the methods for computing the breach parameters. Since the dam breach inundation mapping relies on a tiered approach (with three levels of analysis: basic, intermediate and advanced), the selection of these parameters and of the routing model mainly depends on the hazard and the population at risk. As regards the study area, it is pointed out that it should reach downstream the point where the analysed river debouches either into the sea/larger river/large reservoir (within a few tens of kilometres) or the flow velocities reduce to values of 0.3 m/s or the flow area is inside the normal river boundary. With reference to the numerical modelling, the guide specifies that simplified methods, which require less runtimes, cannot be applied to all cases, whereas full dynamic wave equations (e.g. shallow water equations) fit almost all hydraulic problems and hence should be used for dam breach analyses. The choice of the terrain data and of the roughness coefficient are further analysed. In order to assess hazard to downstream populations and properties, the flood hazard mapping has to represent the maximum water depth, velocity and the inundation duration.

References

ADEPT-Environment Agency, 2019. Flood risk emergency plans for new development.

Arrighi, C., Oumeraci, H., Castelli, F., 2017. Hydrodynamics of pedestrians' instability in floodwaters. Hydrol. Earth Syst. Sci. 21 (1), 515–531.

ASCE/EWRI Task Committee on Dam/Levee Breaching. (2011). Earthen embankment breaching. Journal of hydraulic engineering, 137(12), 1549-1564.

Aureli, F., Maranzoni, A., Mignosa, P., Ziveri, C., 2008. 2D numerical modelling for hydraulic hazard assessment: a dam-break case study. River Flow 2008, Proc. Int. Conf. Fluv. Hydraul. M, 729–736.

Aureli, F., Maranzoni, A., Mignosa, P., 2014. A semi-analytical method for predicting the outflow hydrograph due to dam-break in natural valleys. Adv. Water Resour. 63, 38–44.

Aureli, F., Maranzoni, A., Petaccia, G., 2021. Review of historical dam-break events and laboratory tests on real topography for the validation of numerical models. Water 13 (14), 1968.

Ayoub, V., Delenne, C., Chini, M., Finaud-Guyot, P., Mason, D., Matgen, P., Maria-Pelich, R., Hostache, R., 2022. A porosity-based flood inundation modelling approach for enabling faster large scale simulations. Adv. Water Resour. 162, 104141.

Azeez, O., Elfeki, A., Kamis, A.S., Chaabani, A., 2020. Dam break analysis and flood disaster simulation in arid urban environment: The Um Al-Khair dam case study, Jeddah, Saudi Arabia. Nat. Hazards 100 (3), 995–1011.

Bates, P.D., Horritt, M.S., Fewtrell, T.J., 2010. A simple inertial formulation of the shallow water equations for efficient two-dimensional flood inundation modelling. J. Hydrol. 387 (1–2), 33–45.

Begnudelli, L., Sanders, B.F., 2007. Simulation of the St. Francis dam-break flood. J. Eng. Mech. 133 (11), 1200–1212.

Brodtkorb, A.R., Sætra, M.L., Altinakar, M., 2012. Efficient shallow water simulations on GPUs: Implementation, visualization, verification, and validation. Comput. Fluids 55, 1–12.

Bruschin, J., Bauer, S., Delley, P., Trucco, G., 1982. The overtopping of the Palagnedra dam. Int. Water Power Dam Constr. 34, 13–19.

Cantero-Chinchilla, F.N., Bergillos, R.J., Gamero, P., Castro-Orgaz, O., Cea, L., Hager, W. H., 2020. Vertically averaged and moment equations for dam-break wave modeling: Shallow water hypotheses. Water 12 (11), 3232.

Casas, A., Benito, G., Thorndycraft, V.R., Rico, M., 2006. The topographic data source of digital terrain models as a key element in the accuracy of hydraulic flood modelling. Earth Surf. Process. Landforms J. Brit. Geomorphol. Res. Group 31 (4), 444–456.

Castro, M.J., Ortega, S., De la Asuncion, M., Mantas, J.M., Gallardo, J.M., 2011. GPU computing for shallow water flow simulation based on finite volume schemes. Comptes Rendus Mécanique 339 (2–3), 165–184.

Central Water Commission, 2018. Guidelines for Mapping Flood Risks Associated with Dams, Government of India.

Chen, J., Shi, H., Sivakumar, B., Peart, M.R., 2016. Population, water, food, energy and dams. Renew. Sustain. Energy Rev. 56, 18–28.

Costabile, P., Costanzo, C., Macchione, F., 2017. Performances and limitations of the diffusive approximation of the 2-d shallow water equations for flood simulation in urban and rural areas. Appl. Numer. Math. 116, 141–156.
Costabile, P., Costanzo, C., De Lorenzo, G., Macchione, F., 2020. Is local flood hazard assessment in urban areas significantly influenced by the physical complexity of the hydrodynamic inundation model? J. Hydrol. 580, 124231.
Dazzi, S., Vacondio, R., Dal Palù, A., Mignosa, P., 2018. A local time stepping algorithm for GPU-accelerated 2D shallow water models. Adv. Water Resour. 111, 274–288.
Dazzi, S., Vacondio, R., Mignosa, P., 2019. Integration of a levee breach erosion model in a GPU-accelerated 2D shallow water equations code. Water Resour. Res. 55 (1), 682–702.
Dazzi, S., Shustikova, I., Domeneghetti, A., Castellarin, A., Vacondio, R., 2021. Comparison of two modelling strategies for 2D large-scale flood simulations. Environ. Model. Softw. 146, 105225.
Environment Agency, 2013. Guide to risk assessment for reservoir safety management. Volume 2: Methodology and supporting information.
FEMA, 2013. Federal Guidelines for Inundation Mapping of Flood Risks Associated with Dam Incidents and Failures.
Ferrari, A., D'Oria, M., Vacondio, R., Dal Palù, A., Mignosa, P., Tanda, M.G., 2018. Discharge hydrograph estimation at upstream-ungauged sections by coupling a Bayesian methodology and a 2-D GPU shallow water model. Hydrol. Earth Syst. Sci. 22 (10), 5299–5316.
Ferrari, A., Viero, D.P., Vacondio, R., Defina, A., Mignosa, P., 2019. Flood inundation modeling in urbanized areas: A mesh-independent porosity approach with anisotropic friction. Adv. Water Resour. 125, 98–113.
Ferrari, A., Dazzi, S., Vacondio, R., Mignosa, P., 2020. Enhancing the resilience to flooding induced by levee breaches in lowland areas: a methodology based on numerical modelling. Nat. Hazards Earth Syst. Sci. 20 (1), 59–72.
Ferrari, A., Viero, D.P., 2020. Floodwater pathways in urban areas: A method to compute porosity fields for anisotropic subgrid models in differential form. J. Hydrol. 589, 125193.
Froehlich, D.C., 2008. Embankment dam breach parameters and their uncertainties. J. Hydraul. Eng. 134 (12), 1708–1721.
Furlan, P., Pfister, M., Matos, J., Amado, C., Schleiss, A.J., 2021. Blockage probability modeling of large wood at reservoir spillways with piers. Water Resour. Res. 57 (8) e2021WR029722.
Gaagai, A., Aouissi, H.A., Krauklis, A.E., Burlakovs, J., Athamena, A., Zekker, I., Boudoukha, A., Benaabidate, L., Chenchouni, H., 2022. Modeling and risk analysis of dam-break flooding in a semi-arid montane watershed: A case study of the Yabous Dam, Northeastern Algeria. Water 14 (5), 767.
Hu, P., Lei, Y., Han, J., Cao, Z., Liu, H., He, Z., 2019b. Computationally efficient modeling of hydro-sediment-morphodynamic processes using a hybrid local time step/global maximum time step. Adv. Water Resour. 127, 26–38.
Hu, P., Lei, Y., Han, J., Cao, Z., Liu, H., He, Z., Yue, Z., 2019a. Improved local time step for 2d shallow-water modeling based on unstructured grids. J. Hydraul. Eng. 145 (12), 06019017.
ICOLD, 2020. Dam Legislation: final report.
Juez, C., Lacasta, A., Murillo, J., García-Navarro, P., 2016. An efficient GPU implementation for a faster simulation of unsteady bed-load transport. J. Hydraul. Res. 54 (3), 275–288.
Kakoulaki, G., Martinez, A., & Florio, P. (2021). Non-commercial Light Detection and Ranging (LiDAR) data in Europe.
Khosravi, K., Chegini, A.H.N., Cooper, J., Mao, L., Habibnejad, M., Shahedi, K., Binns, A., 2021. A laboratory investigation of bed-load transport of gravel sediments under dam break flow. Int. J. Sedim. Res. 36 (2), 229–234.
Kostecki, S., Banasiak, R., 2021. The catastrophe of the Niedów Dam—The causes of the dam's breach, its development, and consequences. Water 13 (22), 3254.
Kurganov, A., Petrova, G., 2007. A second-order well-balanced positivity preserving central-upwind scheme for the Saint-Venant system. Commun. Math. Sci. 5 (1), 133–160.
Lacasta, A., Juez, C., Murillo, J., García-Navarro, P., 2015. An efficient solution for hazardous geophysical flows simulation using GPUs. Comput. Geosci. 78, 63–72.
Lazzarin, T., Viero, D.P., Molinari, D., Ballio, F., Defina, A., 2022. Flood damage functions based on a single physics-and data-based impact parameter that jointly accounts for water depth and velocity. J. Hydrol. 607, 127485.
Liang, Q., Borthwick, A.G., 2009. Adaptive quadtree simulation of shallow flows with wet–dry fronts over complex topography. Comput. Fluids 38 (2), 221–234.
Liang, Q., Du, G., Hall, J.W., Borthwick, A.G., 2008. Flood inundation modeling with an adaptive quadtree grid shallow water equation solver. J. Hydraul. Eng. 134 (11), 1603–1610.
Liang, Q., Marche, F., 2009. Numerical resolution of well-balanced shallow water equations with complex source terms. Adv. Water Resour. 32 (6), 873–884.
Marangoz, H.O., Anilan, T., 2022. Two-dimensional modeling of flood wave propagation in residential areas after a dam break with application of diffusive and dynamic wave approaches. Nat. Hazards 110 (1), 429–449.
Maranzoni, A., Mignosa, P., 2019. Seismic-generated unsteady motions in shallow basins and channels. Part II: Numerical modelling. App. Math. Model. 68, 712–731.
Mason, D.C., Horritt, M.S., Dall'Amico, J.T., Scott, T.R., Bates, P.D., 2007. Improving river flood extent delineation from synthetic aperture radar using airborne laser altimetry. IEEE Trans. Geosci. Remote Sens. 45 (12), 3932–3943.
Mason, D.C., Garcia-Pintado, J., Cloke, H.L., Dance, S.L., 2015. The potential of flood forecasting using a variable-resolution global digital terrain model and flood extents from synthetic aperture radar images. Front. Earth Sci. 3, 43.
Meesuk, V., Vojinovic, Z., Mynett, A.E., Abdullah, A.F., 2015. Urban flood modelling combining top-view LiDAR data with ground-view SfM observations. Adv. Water Resour. 75, 105–117.
Mignosa, P., Vacondio, R., Aureli, F., Dazzi, S., Ferrari, A., Prost, F., 2018. High resolution 2D modelling of rapidly varying flows: Some case studies. Ital. J. Eng. Geol. Environ. 2018, 143–160.
Milanesi, L., Pilotti, M., Ranzi, R., 2015. A conceptual model of people's vulnerability to floods. Water Resour. Res. 51 (1), 182–197.
Milanesi, L., Pilotti, M., 2021. Coupling Flood Propagation Modeling and Building Collapse in Flash Flood Studies. J. Hydraul. Eng. 147 (12), 04021047.
Néelz, S., Pender, G., Villanueva, I., Wilson, M., Wright, N.G., Bates, P., Mason, D., Whitlow, C., 2006. Using remotely sensed data to support flood modelling. Proc. Inst. Civ. Eng. Water Manag. 159 (1), 35–43.
Persi, E., Meninno, S., Petaccia, G., Sibilla, S., Armanini, A., 2022. Modeling Large Wood Transport in Semi-Congested Regime with Multiple Entry Points. Water 14 (3), 421.
Petaccia, G., Lai, C.G., Milazzo, C., Natale, L., 2016. The collapse of the Sella Zerbino gravity dam. Eng. Geol. 211, 39–49.
Pilotti, M., Maranzoni, A., Tomirotti, M., Valerio, G., 2011. 1923 Gleno dam break: Case study and numerical modeling. J. Hydraul. Eng. 137 (4), 480–492.
Sætra, M.L., Brodtkorb, A.R., Lie, K.A., 2015. Efficient GPU-implementation of adaptive mesh refinement for the shallow-water equations. J. Sci. Comput. 63 (1), 23–48.
Sanders, B.F., 2008. Integration of a shallow water model with a local time step. J. Hydraul. Res. 46 (4), 466–475.
Sanders, B.F., Schubert, J.E., Detwiler, R.L., 2010. ParBreZo: A parallel, unstructured grid, Godunov-type, shallow-water code for high-resolution flood inundation modeling at the regional scale. Adv. Water Resour. 33 (12), 1456–1467.
Sarchani, S., Koutroulis, A.G., 2022. Probabilistic dam breach flood modeling: the case of Valsamiotis dam in Crete. Nat. Hazards 114 (2), 1763–1814.
Schubert, J.E., Sanders, B.F., 2012. Building treatments for urban flood inundation models and implications for predictive skill and modeling efficiency. Adv. Water Resour. 41, 49–64.
Smith, N.A., 2017. The failure of the Bouzey dam in 1895. Dams.
Soares-Frazão, S., Canelas, R., Cao, Z., Cea, L., Chaudhry, H.M., Die Moran, A., El Kadi, K., Ferreira, R., Cadórniga, I.F., Gonzalez-Ramirez, N., Greco, M., Huang, W., Imran, J., Le Coz, J., Marsooli, R., Paquier, A., Pender, G., Pontillo, M., Puertas, J., Spinewine, B., Swartenbroekx, C., Tsubaki, R., Villaret, C., Wu, W., Yue, Z., Zech, Y., 2012. Dam-break flows over mobile beds: Experiments and benchmark tests for numerical models. J. Hydraul. Res. 50 (4), 364–375.
Toro, E. F. (2001). Shock-Capturing Methods for Free-Surface Shallow Flows, ed John Wiley & Sons.
Urzică, A., Mihu-Pintilie, A., Stoleriu, C.C., Cîmpianu, C.I., Huţanu, E., Pricop, C.I., Grozavu, A., 2021. Using 2D HEC-RAS modeling and embankment dam break scenario for assessing the flood control capacity of a multi-reservoir system (NE Romania). Water 13 (1), 57.
Vacondio, R., Mignosa, P., Pagani, S., 2013. 3D SPH numerical simulation of the wave generated by the Vajont rockslide. Adv. Water Resour. 59, 146–156.
Vacondio, R., Dal Palù, A., Mignosa, P., 2014. GPU-enhanced finite volume shallow water solver for fast flood simulations. Environ. Model. Softw. 57, 60–75.
Vacondio, R., Aureli, F., Ferrari, A., Mignosa, P., Dal Palu, A., 2016. Simulation of the January 2014 flood on the Secchia River using a fast and high-resolution 2D parallel shallow-water numerical scheme. Nat. Hazards 80 (1), 103–125.
Vacondio, R., Dal Palù, A., Ferrari, A., Mignosa, P., Aureli, F., Dazzi, S., 2017. A non-uniform efficient grid type for GPU-parallel Shallow Water Equations models. Environ. Model. Softw. 88, 119–137.
Valiani, A., Caleffi, V., Zanni, A., 2002. Case study: Malpasset dam-break simulation using a two-dimensional finite volume method. J. Hydraul. Eng. 128 (5), 460–472.
Verma, S., Patra, K.C., 2022. Dam break flow simulation model for preparing emergency action plans for Bargi Dam failure. In: Hydrological Modeling. Springer, Cham, pp. 271–286.
Xia, J., Lin, B., Falconer, R.A., Wang, G., 2010. Modelling dam-break flows over mobile beds using a 2D coupled approach. Adv. Water Resour. 33 (2), 171–183.
Xu, Y., Zhang, L.M., 2009. Breaching parameters for earth and rockfill dams. J. Geotech. Geoenviron. Eng. 135 (12), 1957–1970.
Zarfl, C., Lumsdon, A.E., Berlekamp, J., Tydecks, L., Tockner, K., 2015. A global boom in hydropower dam construction. Aquat. Sci. 77 (1), 161–170.
Zhou, X., Chen, Z., Yu, S., Wang, L., Deng, G., Sha, P., Li, S., 2015. Risk analysis and emergency actions for Hongshiyan barrier lake. Nat. Hazards 79 (3), 1933–1959.
Zhou, X., Chen, Z., Zhou, J., Guo, X., Du, X., Zhang, Q., 2020. A quantitative risk analysis model for cascade reservoirs overtopping: principle and application. Nat. Hazards 104 (1), 249–277.